The Astrophysical Journal, 973:149 (16pp), 2024 October 1 https://doi.org/10.3847/1538-4357/ad67ca

Effects of Multichannel Active Galactic Nuclei Feedback in FIRE Cosmological Simulations of Massive Galaxies

Lindsey Byrne[1], Claude-André Faucher-Giguère[1], Sarah Wellons[2], Philip F. Hopkins[3], Daniel Anglés-Alcázar[4,5], Imran Sultan[1], Nastasha Wijers[1], Jorge Moreno[5,6], and Sam Ponnada[3]
[1] Department of Physics and Astronomy and CIERA, Northwestern University, Evanston, IL 60201, USA; byrnelin@u.northwestern.edu
[2] Department of Astronomy, Van Vleck Observatory, Wesleyan University, 96 Foss Hill Drive, Middletown, CT 06459, USA
[3] California Institute of Technology, TAPIR, Mailcode 350-17, Pasadena, CA 91125, USA
[4] Department of Physics, University of Connecticut, 196 Auditorium Road, U-3046, Storrs, CT 06269-3046, USA
[5] Center for Computational Astrophysics, Flatiron Institute, 162 Fifth Avenue, New York, NY 10010, USA
[6] Department of Physics and Astronomy, Pomona College, Claremont, CA 91711, USA
Received 2023 October 21; revised 2024 July 22; accepted 2024 July 24; published 2024 September 27

Abstract

Feedback from supermassive black holes is believed to be a critical driver of the observed color bimodality of galaxies above the Milky Way mass scale. Active galactic nuclei (AGN) feedback has been modeled in many galaxy formation simulations, but most implementations have involved simplified prescriptions or a coarse-grained interstellar medium (ISM). We present the first set of Feedback In Realistic Environments (FIRE)-3 cosmological zoom-in simulations with AGN feedback evolved to $z \sim 0$, examining the impact of AGN feedback on a set of galaxies with halos in the mass range 10^{12}–$10^{13}\,M_{\odot}$. These simulations combine detailed stellar and ISM physics with multichannel AGN feedback including radiative feedback, mechanical outflows, and, in some simulations, cosmic rays (CRs). We find that massive ($>L^{*}$) galaxies in these simulations can match local scaling relations including the stellar mass–halo mass relation and the $M_{\rm BH}$–σ relation; in the stronger model with CRs, they also match the size–mass relation and the Faber–Jackson relation. Many of the massive galaxies in the simulations with AGN feedback have quenched star formation and elliptical morphologies, in qualitative agreement with observations. In contrast, simulations at the massive end without AGN feedback produce galaxies that are too massive and form stars too rapidly, are order-of-magnitude too compact, and have velocity dispersions well above Faber–Jackson. Despite these successes, the AGN models analyzed do not produce uniformly realistic galaxies when the feedback parameters are held constant: While the stronger model produces the most realistic massive galaxies, it tends to overquench the lower-mass galaxies. This indicates that further refinements of the AGN modeling are needed.

Unified Astronomy Thesaurus concepts: Supermassive black holes (1663); Active galactic nuclei (16); Galaxy quenching (2040); AGN host galaxies (2017); Galaxy evolution (594); Hydrodynamical simulations (767)

1. Introduction

Over the past two decades, observations of galaxies hosting luminous quasars have found wide-angle, kiloparsec-scale, multiphase outflows (Moe et al. 2009; Feruglio et al. 2010; Fischer et al. 2010; Fabian 2012; Liu et al. 2013; Rupke & Veilleux 2013; Fiore et al. 2017). These outflows provide crucial evidence for the impact of active galactic nuclei (AGN) on their host galaxies: The outflow rates can exceed the galaxy's star formation rate (SFR), and the energetics of the outflows are correlated to the luminosity of the AGN (Sturm et al. 2011; Cicone et al. 2014). Other properties of supermassive black holes (SMBHs) have also been demonstrated to correlate with properties of their host galaxies, including scaling relations between black hole (BH) mass and stellar velocity dispersion and between BH mass and stellar bulge mass (Magorrian et al. 1998; Ferrarese & Merritt 2000; Gebhardt et al. 2000). These scaling relations indicate that BHs and galaxies develop together. This coevolution can likely be explained through the feedback energy produced by accretion onto the SMBH (Silk & Rees 1998; Di Matteo et al. 2005; Hopkins et al. 2007). In addition to driving winds, observational evidence suggests that AGN can heat the interstellar/circumgalactic/intracluster medium (ISM/CGM/ICM) with powerful, relativistic jets (Fabian 2012).

Feedback from SMBHs is thought to be key to understanding how galaxies quench, or stop actively forming stars (Di Matteo et al. 2005; Springel et al. 2005; Sijacki et al. 2007). Substantial observational evidence indicates that star formation becomes increasingly likely to cease in galaxies above a stellar mass of approximately $10^{10.5}\,M_{\odot}$, corresponding to a halo mass $M_{\rm halo} \sim 10^{12}\,M_{\odot}$, creating a population of "red and dead" massive galaxies (Peng et al. 2010; Muzzin et al. 2013; Tomczak et al. 2014). Understanding the physical processes that lead to this quenching is a key question in galaxy formation theory. While several possible hypotheses have been proposed, feedback from AGN has emerged as a leading candidate, with many studies showing that without AGN feedback, simulations fail to reproduce the observed galaxy mass function (Somerville et al. 2008; Harrison 2017) and massive galaxy properties (e.g., Su et al. 2019; Wellons et al. 2020; Parsotan et al. 2021; Cochrane et al. 2023).

As the physics of SMBH accretion and feedback occurs on scales below the resolution of typical cosmological simulations, it is necessary to rely on subgrid models. However, much uncertainty remains as to how best to represent the physics

involved due to open questions about the fundamental physics. Various forms of AGN feedback—including various combinations of thermal energy injection, winds, and jets—have been implemented as subgrid models in galaxy formation simulations (see reviews in Somerville & Davé 2015; Naab & Ostriker 2017; Crain & Voort 2023; Di Matteo et al. 2023). In addition to reproducing scaling relations, cosmological simulations with AGN feedback have demonstrated success in quenching star formation and producing quiescence in massive galaxies (e.g Schaye et al. 2015; Dubois et al. 2016; Tremmel et al. 2017; Davé et al. 2019; Rosito et al. 2021). Such simulations have found that AGN feedback can turn star-forming disk galaxies into quenched early-type galaxies by expelling gas from the galaxy, preventing the cooling of gas in the CGM, and reducing in situ star formation (Davies et al. 2020; Terrazas et al. 2020).

The large-volume cosmological simulations generally utilize coarse-grained treatments of the ISM with baryonic mass resolutions in the range $m_b \sim 10^5$–$10^7\,M_\odot$, and BH models consisting of phenomenological prescriptions tuned to produce galaxy properties that match galaxy-scale observations. Another approach is to simulate massive galaxies at much higher resolution and with more explicit small-scale physics, but to omit the cosmological setting. Simulations of isolated massive ellipticals with AGN feedback of this type, such as those reported by, for example, Ciotti & Ostriker (2007), Ciotti et al. (2010, 2022), Su et al. (2019), and Yoon et al. (2019), have also produced promising results with regards to reproducing the properties of massive galaxies. An intermediate approach is to use the "zoom-in" technique, which allows simulations to include full cosmological evolution but concentrate the resolution on halos of special interest. In principle, this allows the modeling of more detailed physics while retaining the cosmological context. Zoom-in simulations have also been used with significant success to simulate the effects of AGN feedback on the formation of massive galaxies (e.g., Dubois et al. 2013; Choi et al. 2017, 2018, 2020, 2024; Frigo et al. 2019). However, most previously published cosmological zoom-in simulations of massive galaxies still have relatively coarse baryonc mass resolutions $m_b \gtrsim 10^6\,M_\odot$ and limited sets of physical processes included.

In this paper, we build on previous work and use cosmological zoom-in simulations of galaxy formation from the Feedback In Realistic Environments (FIRE) project to investigate the impact of multichannel AGN feedback in relatively massive galaxies with halos in the mass range of 10^{12}–$10^{13}\,M_\odot$.[7] These correspond to Milky Way–mass ($\sim L^*$) galaxies and intermediate-mass ($>L^*$) elliptical galaxies. In contrast to most large-volume simulations, the high resolution of the FIRE simulations allows us to resolve the multiphase nature of the ISM and more accurately capture interactions between AGN feedback and the ISM. All simulations are evolved using the FIRE-3 code (Hopkins et al. 2023). FIRE-3 represents an update from FIRE-2 (Hopkins et al. 2018), including updates to the treatment of stellar evolution physics, nucleosynthetic yields, and low-temperature ISM cooling. Additionally, we use a detailed, multichannel AGN feedback model which combines multiple forms of radiative feedback (e.g., radiation pressure, photoionization, and Compton heating) with kinetic outflows and, in some simulations, cosmic rays (CRs). Our highest-resolution simulations at the Milky Way–mass scale have a baryonic particle mass $m_b \approx 7000\,M_\odot$ and our highest-resolution runs for $>L^*$ galaxies have $m_b \approx 3 \times 10^4\,M_\odot$. These resolutions are higher than even most previously published cosmological zoom-in simulations including AGN feedback at those mass scales, and the set of feedback mechanisms explicitly modeled is more complete than those used in most previous cosmological simulations.

Our new cosmological simulations expand previous, more idealized studies of AGN feedback by our team in analytic models (Faucher-Giguère & Quataert 2012; Faucher-Giguère et al. 2012; Richings & Faucher-Giguère 2018) and idealized simulations (Richings & Faucher-Giguère 2018; Richings et al. 2021) of AGN winds, as well as in simulations including the FIRE ISM physics but neglecting the cosmological environment (Hopkins et al. 2016; Torrey et al. 2020). This work is complementary to Mercedes-Feliz et al. (2023, 2024) and Cochrane et al. (2023), which analyzed the impact of AGN winds during a luminous quasar phase in a massive FIRE-2 star-forming galaxy, and to Wellons et al. (2023), which explored the impact of various models of SMBH accretion and feedback in a large suite of FIRE-2 simulations and found several physically plausible models. We apply AGN feedback models broadly consistent with those favored by Wellons et al. (2023) to a suite of cosmological zoom-in simulations with updated FIRE-3 physics. Moreover, about half of our new simulations are of order-of-magnitude higher mass resolution than the simulations of comparable-mass galaxies studied in Wellons et al. (2023).

We examine the impact of AGN feedback in the FIRE simulations by making a detailed comparison between two possible models for AGN feedback, simulations without BHs, and observations. Our study builds on Wellons et al. (2023) by comparing the simulations to a broader set of observations, including more detailed structural properties. We present a set of massive ($>L^*$), quenched galaxies that broadly match observed scaling relations at low redshifts. Along with some of the FIRE-2 test simulations studied by Wellons et al. (2023), these constitute the first such galaxies produced in cosmological simulations by the FIRE project. While we show examples of how including AGN feedback in simulations of massive galaxies produces much more realistic properties than simulations without BHs, we also highlight significant limitations of the AGN models analyzed in this paper. In particular, we find that while the stronger variant (with CRs included) produces the most realistic $>L^*$ galaxies, it tends to overquench lower-mass galaxies. Thus, we find evidence that further refinements of the BH growth and/or feedback physics—perhaps including feedback parameters that depend on galaxy mass—are warranted. The parameter space of possible SMBH feeding and feedback is vast, and, as our results reinforce, continues to require more exploration.

The plan for this paper is as follows. In Section 2, we describe the suite of zoom-in simulations analyzed for this study, along with the three SMBH physics models tested. In Section 3, we present the outcomes of the simulations with comparisons to observations of galaxy masses and SFRs (Section 3.2) and structural properties (Section 3.3). In Section 4, we discuss our results, and in Section 5, we summarize our conclusions.

Throughout, we assume a standard flat Lambda cold dark matter (ΛCDM) cosmology, with matter density $\Omega_m \approx 0.3$,

[7] See the FIRE project website: http://fire.northwestern.edu.

Table 1
BH Feedback Parameters and Energetics for the Physics Models Compared in This Paper

Parameter	NoBH	BH	BH+CR
$v_{\rm wind}$ (km s^{-1})	···	3000	3000
$\epsilon_{\rm wind}^{\rm BH}$	···	5.0×10^{-5}	5.0×10^{-5}
$\epsilon_{\rm rad}^{\rm BH}$	···	0.1	0.1
$\epsilon_{\rm CR}^{\rm BH}$	···	···	10^{-3}

Note. $v_{\rm wind}$ is the velocity of mechanical winds, $\epsilon_{\rm wind}^{\rm BH}=(v_{\rm wind}/c)^2/2$ defines the energy going into winds (Equation (7)), $\epsilon_{\rm rad}^{\rm BH}$ is the radiative efficiency (Equation (6)), and $\epsilon_{\rm CR}$ defines the energy injected in CRs (Equation (8)).

baryon density $\Omega_{\rm b}\approx0.05$, dark energy density $\Omega_\Lambda\approx0.7$, and Hubble constant $H_0\approx70\,{\rm km\,s^{-1}\,Mpc^{-1}}$, consistent with recent measurements (Planck Collaboration et al. 2020).[8]

2. Methods

2.1. FIRE Simulations

We analyze a set of FIRE-3 cosmological zoom-in simulations, all of which were run with the hydrodynamics code GIZMO in meshless finite mass mode (Hopkins 2015).[9] Details of the FIRE-3 methods and physics are explained in Hopkins et al. (2023). The simulations include all standard FIRE-3 physics, including multiple forms of stellar feedback, including feedback from supernovae of Type I and II, stellar winds from OB and asymptotic giant branch stars, photoionization, and radiation pressure. Star formation occurs in dense, self-gravitating gas. The high resolution of these simulations allows us to resolve the multiphase ISM. All simulations include magnetic fields, using the magnetohydrodynamics methods described in Hopkins & Raives (2016) and Hopkins (2016).

Our simulation suite consists of 16 sets of initial conditions: seven Milky Way–mass galaxies with final halo mass $M_{\rm halo}\sim10^{12}\,M_\odot$ (which we hereafter refer to as "m12" galaxies), and nine galaxies reaching $M_{\rm halo}\sim10^{13}\,M_\odot$ at $z=0$ (which we hereafter refer to as "m13" galaxies). Note that while we will refer to the m13 galaxies as "massive" in comparison to the Milky Way–mass galaxies, they are what would generally be considered intermediate mass relative to $>L^*$ ellipticals. As shown in Table 2, each set of initial conditions is evolved with between one and three physics models. The three primary models we analyze for this paper are as follows: one without any SMBHs at all, one which models BHs with both radiative and mechanical feedback, and one with both BHs and CR physics. These models, which we hereafter refer to as the "NoBH," "BH," and "BH+CR" models, are described in more detail below and defined by the parameters in Table 1. Four sets of initial conditions, two m12s and two m13s, were evolved with all three of these models; these galaxies are bolded in Table 2.

We tested a range of mass resolutions, from a baryonic mass of $m_{\rm b}=7\times10^3\,M_\odot$ for our highest-resolution simulations to a baryonic mass of $m_{\rm b}=3\times10^5\,M_\odot$ for our lowest-resolution simulations. Simulations of higher-mass galaxies, or which include the expensive CR model, are run with lower resolution. Wellons et al. (2023) investigated resolution effects when examining similar FIRE simulations, also including AGN physics. These authors found that, while there is some resolution dependence of the results, the qualitative conclusions are not affected for the range of resolutions studied here.

The final redshift is $z=0$ for most of the simulations, with a few ending at redshifts of $z\sim0.1$ or $z\sim0.2$; for simplicity, we refer to this range as $z\sim0$ throughout our analysis. These minor differences in final redshift are because in some cases evolving the simulations to $z=0$ is prohitively computationally expensive. This occurs in some massive galaxies without AGN feedback, which can develop extremely dense stellar cores when they fail to quench, and in our highest-resolution simulations of massive galaxies. While this introduces some heterogeneity to our data set, it does not affect our overall conclusions. We note that high-resolution galaxy formation simulations like ours are subject to substantial stochastic effects (e.g., the exact timing of bursts of star formation or AGN activity), so we could not robustly compare detailed galaxy properties between matching runs even if they were all uniformly evolved to $z=0$.

Although not the focus of this paper, we additionally considered a "NoBH+CR" model with CRs from stellar sources but without AGN feedback (noBH+CR). We have one m12 run (m12i) and one m13 run (m13h206) with this model. However, we were unable to evolve the m13 run to $z\sim0$, as the galaxy became unphysically dense and compact without AGN feedback. When overly dense stellar cores develop, the simulations often become prohibitively expensive to evolve due to the short time steps required in dense regions, and this is even more so when the CR solver is enabled. The m13h206 NoBH+CR run became too computationally expensive to integrate past $z=0.5$. Since we only have one simulation at each mass scale with the NoBH+CR model, and due to stochasticity, we cannot draw robust conclusions from comparing most diagnostics on these runs to the other models. We therefore do not include these runs in most of our comparisons below, but we return to them in Section 4.2 on the effects of CRs. As we explain there, the effects on stellar sizes is one relatively robust diagnostic because once a massive simulated galaxy becomes an order of magnitude too compact (interpreted as being due to the feedback being too weak), it is highly unlikely that the galaxy would recover realistic properties by evolving the simulation longer.

A note about the FIRE-3 simulations discussed in this study: One technical improvement in FIRE-3 (relative to FIRE-2) is the adoption of a "velocity-aware" technique for energy and momentum distribution to nearby gas particles in modeling supernova feedback (as described in Hopkins et al. 2023). This approach improves conservation properties when the ambient gas is not static. However, as P. F. Hopkins et al. (2024, in preparation) shows, this approach does not uniquely specify how much momentum should be deposited following unresolved supernova feedback events treated in subgrid. A particular choice was made in the implementation described in the original FIRE-3 methods paper and in the simulations in this paper. Although this was not highlighted in the original

[8] In detail, the cosmological parameters in our simulations vary slightly depending on initial conditions: $\Omega_{\rm m}=0.272$–0.310, $\Omega_{\rm b}=0.0455$–0.0486, $\Omega_\Lambda=0.691$–0.728, and $H_0=67.8$–$70.2\,{\rm km\,s^{-1}\,Mpc^{-1}}$. These minor variations do not affect our conclusions.

[9] See the GIZMO project website: http://www.tapir.caltech.edu/~phopkins/Site/GIZMO.html.

Table 2
Parameters of the FIRE-3 Simulation Suite Analyzed in This Work

Halo	Model	Final z	Halo Mass ($M_\odot$)	Stellar Mass ($M_\odot$)	m_b ($M_\odot$)	ϵ_{star} (pc)
m12f	NoBH	0.00	1.2×10^{12}	1.5×10^{10}	7×10^3	5
	BH	0.00	1.1×10^{12}	1.5×10^{10}	7×10^3	10
	BH+CR	0.00	1.0×10^{12}	8.6×10^9	6×10^4	10
m12q	NoBH	0.00	1.4×10^{12}	3.5×10^{10}	7×10^3	5
	BH	0.20	1.1×10^{12}	1.4×10^{10}	7×10^3	5
	BH+CR	0.00	1.2×10^{12}	7.1×10^9	6×10^4	10
m12b	BH	0.00	1.1×10^{12}	2.1×10^{10}	7×10^3	5
m12i	NoBH+CR	0.00	8.8×10^{11}	2.5×10^{10}	6×10^4	10
	BH	0.00	8.6×10^{11}	1.4×10^{10}	7×10^3	5
	BH+CR	0.00	7.8×10^{11}	10.0×10^9	6×10^4	10
m12m	BH	0.00	1.3×10^{12}	4.5×10^{10}	7×10^3	5
	BH+CR	0.00	9.4×10^{11}	1.6×10^{10}	6×10^4	10
m12r	NoBH	0.00	8.6×10^{11}	7.9×10^9	7×10^3	5
	BH	0.00	8.9×10^{11}	8.8×10^9	7×10^3	5
m12w	NoBH	0.00	8.6×10^{11}	9.2×10^9	7×10^3	5
	BH	0.00	8.9×10^{11}	1.4×10^{10}	7×10^3	5
m13h113	NoBH	0.00	9.1×10^{12}	4.6×10^{11}	3×10^5	18
	BH	0.08	8.1×10^{12}	1.7×10^{11}	3×10^4	8
	BH+CR	0.00	6.9×10^{12}	8.9×10^{10}	3×10^5	18
m13h206	NoBH	0.00	6.7×10^{12}	3.3×10^{11}	3×10^5	18
	NoBH+CR	0.50	6.2×10^{12}	5.0×10^{10}	3×10^5	18
	BH	0.20	5.8×10^{12}	1.4×10^{11}	3×10^4	8
	BH+CR	0.00	5.7×10^{12}	5.2×10^{10}	3×10^5	18
m13h002	BH+CR	0.00	2.0×10^{13}	9.6×10^{10}	3×10^5	18
m13h007	NoBH	0.00	2.3×10^{13}	6.4×10^{11}	3×10^5	18
	BH+CR	0.00	2.0×10^{13}	1.5×10^{11}	3×10^5	18
m13h009	BH+CR	0.00	2.8×10^{13}	8.0×10^{10}	3×10^5	18
m13h029	NoBH	0.14	1.4×10^{13}	6.2×10^{11}	3×10^5	18
	BH+CR	0.00	1.1×10^{13}	1.2×10^{10}	3×10^5	18
m13h037	BH+CR	0.00	2.0×10^{13}	1.3×10^{11}	3×10^5	18
m13h223	NoBH	0.06	4.1×10^{13}	9.4×10^{11}	3×10^5	18
m13h236	NoBH	0.20	8.9×10^{12}	3.2×10^{11}	3×10^5	18
	BH+CR	0.00	1.5×10^{13}	6.7×10^{10}	3×10^5	18

Notes. Milky Way–mass halos ("m12s") are listed in the upper half of the table, and massive galaxies ("m13s") are listed in the lower half. Bolded simulations are those for which the initial conditions were run with all three primary physics models discussed in this paper. Columns are as follows: physics model, final redshift, halo mass and stellar mass at the final redshift, the baryonic mass resolution m_b, and the stellar gravitational softening length ϵ_{star} in physical units.

FIRE-3 methods paper, this implementation implies a relatively large supernova momentum injection in converging flows.[10] In particular, converging flows result in an average supernova momentum injection that is higher in the FIRE-3 runs than in FIRE-2 runs. Even before AGN feedback is enabled, this leads to smaller galaxy stellar masses in massive halos compared to FIRE-2 (Hopkins et al. 2023). Since there remains significant uncertainties in the "correct" terminal supernova momentum to use in subgrid models and the FIRE-3 velocity-aware deposition scheme does not uniquely specify how to model it, future FIRE-3 runs will explore and use variations. Thus, some results may differ in future variants of FIRE-3 runs.

[10] This can be understood as the energy of the pre-supernova converging flow contributing to the outward kinetic energy post-supernova.

For each simulation snapshot, we define the halo center using the "shrinking sphere" method of Power et al. (2003) to find the iterative center of mass of the star particles in the zoom-in region. Throughout this work, we consider the virial radius R_{vir} to be R_{200c}, the radius which encloses a sphere whose average density is 200 times the critical density. We consider the halo mass M_{halo} to be M_{200c}, the total mass within that region.

2.2. Black Hole Physics

In simulations that include BHs, the BH seeding, dynamics, accretion, and feedback follow the methods described in Hopkins et al. (2023). BHs are probabilistically generated from gas cells and form preferentially in areas of high surface

density and low metallicity. The gravitational torque-driven accretion model used in these simulations depends weakly on BH mass. The final BH masses are dominated by the accreted mass and insensitive to the initial seed mass (Anglés-Alcázar et al. 2013, 2017a, 2017b); for these simulations, all BH seeds have initial mass $M_{\rm seed} = 100\,M_\odot$. On average, one BH will seed per M_0 stellar mass, with $M_0 = (1\text{–}3) \times 10^6\,M_\odot$. They move under the influence of gravity, and following the method in Wellons et al. 2023, are artificially accelerated toward the local particle with the highest binding energy, which encourages them to move toward the center of the galaxy. If two BH particles become gravitationally bound to one another within the same interaction kernel, and have overlapping force softenings, they merge within a single time step.

Each BH, with mass $M_{\rm BH}$, is surrounded by a subgrid accretion disk of mass $M_{\rm acc}$. Gas from the accretion kernel, which includes the 256 nearest gas resolution elements up to a maximum radius of 5 kpc, accretes onto the disk at a rate

$$\dot{M}_{\rm acc} = \eta_{\rm acc}(1 - f_{w,*})\,M_{\rm gas}\,\Omega, \tag{1}$$

where the efficiency parameter

$$\eta_{\rm acc} \equiv \frac{0.01[(M_{\rm BH} + M_{\rm acc})/M_{\rm disk}]^{1/6}}{1 + 3(M_{\rm gas}/M_{\rm disk})(M_{\rm disk}/10^9\,M_\odot)^{1/3}} \tag{2}$$

is calibrated from high-resolution simulations to represent the effects of gravitational torques, which lead to angular momentum loss for gas in the galaxy's nucleus and drive gas toward the BH (Hopkins & Quataert 2011; Anglés-Alcázar et al. 2017a, 2017b, 2021). The gas mass $M_{\rm gas}$, galaxy disk mass $M_{\rm disk}$, and dynamical frequency $\Omega = \sqrt{GM_{\rm enc,tot}}/R^3$ are evaluated within the radius of the accretion kernel. $M_{\rm disk}$ is the total mass of gas and stars supported by angular momentum within the accretion kernel, and is estimated following Hopkins & Quataert (2011) by decomposing the stars in the accretion kernel into isotropic and thin-disk components based on their angular momentum. The parameter

$$f_{w,*} \equiv \left[1 + \frac{\bar{a}_{\rm grav}}{\langle \dot{p}_*/m_* \rangle}\right]^{-1} \tag{3}$$

is a correction for gas lost by ejection from stellar feedback (Hopkins et al. 2022c), where $\bar{a}_{\rm grav}$ is the gravitational acceleration inwards and $\langle \dot{p}_*/m_* \rangle \sim 10^{-7}\,{\rm cm\,s^{-2}}$ is the the momentum flux per unit mass from stellar feedback.

The rate at which the BH accretes from the accretion disk, $\dot{M}_{\rm BH}$, is determined following a Shakura & Sunyaev (1973)–like α-disk subgrid prescription:

$$\dot{M}_{\rm BH} \equiv \frac{M_{\rm acc}}{t_{\rm acc}}, \tag{4}$$

where, in our simulations,

$$t_{\rm acc} \equiv 42\ {\rm Myr}\left[1 + \frac{M_{\rm BH}}{M_{\rm acc}}\right]^{0.4}. \tag{5}$$

This effectively smooths the BH accretion rate and allows the feedback to persist after it begins to clear the nucleus.

Accreting BHs inject energy into their surroundings in the forms of radiative and mechanical feedback. Radiative feedback includes radiation pressure, photoionization, and Compton heating. Radiation transport is modeled using the same numerical methods as is used for stellar radiative feedback in the FIRE simulations (Hopkins et al. 2020b). The accretion disk emits radiation with a bolometric luminosity of

$$\dot{E}^{\rm BH}_{\rm rad} \equiv L_{\rm bol} = \epsilon^{\rm BH}_{\rm rad}\,\dot{M}_{\rm BH}c^2, \tag{6}$$

where $\epsilon^{\rm BH}_{\rm rad} = 0.1$, and the total photon momentum flux is $\dot{p}_{\rm rad} = L_{\rm abs}/c$, where $L_{\rm abs}$ is the absorbed photon luminosity in a given gas element. The total momentum deposited by radiation in the ISM in these simulations is typically $\sim L_{\rm bol}/c$ because single scattering dominates.

Mechanical winds are modeled by the spawning of new resolution elements, or wind cells, in the vicinity of the BH (see also Richings & Faucher-Giguère 2018; Torrey et al. 2020; Su et al. 2021; Cochrane et al. 2023; Mercedes-Feliz et al. 2023, 2024). These cells, which have masses of $100\,M_\odot$ (for m12 halos) or $400\,M_\odot$ (for m13 halos), are launched with a total mass outflow rate $\dot{M}_{\rm wind} = \dot{M}_{\rm BH}$ and a velocity of $v_{\rm wind} = 3000\,{\rm km\,s^{-1}}$, generating kinetic energy

$$\dot{E}^{\rm BH}_{\rm wind} = \dot{M}_{\rm BH}\,v^2_{\rm wind}/2 = \epsilon^{\rm BH}_{\rm wind}\,\dot{M}_{\rm BH}c^2, \tag{7}$$

where $\epsilon^{\rm BH}_{\rm wind} = (v_{\rm wind}/c)^2/2 \approx 5 \times 10^{-5}$. The outflows are initially jet-like, collimated along the angular momentum axis of the BHs at the point of injection, though after meeting the ISM and shock heating, they tend to spread along paths of least resistance, with wide solid-angle coverage.

2.3. Cosmic-Ray Feedback

We also test the impact of CR feedback. The NoBH and BH models do not include any CRs. In the "BH+CR model, CRs are injected from both stellar and BH sources.

The simulations with CRs use methods previously reported in detail in previous FIRE papers (Hopkins et al. 2021, 2022a, 2022b). We summarize key elements here. We stress upfront, however, that while the CR treatment is rather complex, this is by no means a "unique" or "final" model of CR feedback, as the uncertainties remain large. Instead, for the purpose of this study, we use this CR model mainly as one stronger variant of the feedback model.

Most previous galaxy formation simulations that have included CRs, including previous FIRE simulations (Chan et al. 2019; Hopkins et al. 2020a, 2021), have used a "single-bin" treatment in which CRs are represented as a second fluid with relativistic energy density in a single effective energy bin. Furthermore, most of these simulations have assumed that the CRs diffuse in space following a prescribed diffusion coefficient κ that is constant in space and in time.

The CR runs in this paper relax both the single-bin and constant κ assumptions. The runs explicitly evolve a CR distribution function (DF) $f(\boldsymbol{x}, \boldsymbol{p}, t, s, \ldots)$ as a function of position $\boldsymbol{x}$, CR momentum $\boldsymbol{p}$, time t, and CR species s, using the algorithm described in Hopkins et al. (2021). This moments-based method uses a closure akin to the M1 closure in radiation hydrodynamics and assumes that the DF is gyrotropic. The momentum-space evolution is integrated in every resolution element using the finite-momentum-space-volume method from Girichidis et al. (2020).

The runs in this paper evolve a CR network consisting of protons, electrons, and positrons. The injection of CRs models unresolved first-order Fermi acceleration at reverse shocks driven by mechanical feedback from SNe, stellar winds and (if

applicable) AGN outflows. Specifically, CRs are injected with an initial spectrum of CR momentum $dj \propto p^{-4.2} d^3\boldsymbol{p}$, where dj is the CR injection rate in an infinitesimal momentum-volume element. The injection spectra are normalized such that 10% of the initial (pre-shock) kinetic energy of the stellar feedback ejecta goes into protons and 2% into leptons, consistent with theoretical models and empirical constraints on CR acceleration. For AGN feedback, if applicable, CRs are injected with an efficiency parameterized by a total energy injection rate (in the same ratio for protons and leptons)

$$\dot{E}_{\rm CR}^{\rm BH} = \epsilon_{\rm CR}^{\rm BH}\, \dot{M}_{\rm BH} c^2, \tag{8}$$

where $\epsilon_{\rm CR}^{\rm BH} = 10^{-3}$ for our runs.

The network includes numerous CR loss/gain terms, described in detail in Hopkins et al. (2022a). These include diffusive reacceleration and adiabatic, gyro-resonant, Coulomb, ionization, hadronic, annihilation, bremsstrahlung, inverse Compton, and synchrotron loss terms.

Crucially, the CRs scatter off unresolved small-scale magnetic inhomogeneities and this drives their transport. This is what is usually modeled using a constant diffusion coefficient in galaxy formation simulations. In the simulations analyzed here, CR transport is instead predicted by evolving their DF assuming a model for the scattering coefficients, which in general depend on local plasma properties. How this is done is described in detail in Hopkins et al. (2022b). Briefly, we adopt the modified external driving model described in Section 5.3.2 of Hopkins et al. (2022b), which is calibrated to reproduce Voyager and AMS-02 CR measurements from MeV to TeV energies in Milky Way–like simulations. This starts with an implementation of a "reference model," which represents a theoretical understanding of how "self-confinement" (SC) and "extrinsic turbulence" (ET) effects developed drive CR scattering, e.g., in Zweibel (2013), Ruszkowski et al. (2017), Zweibel (2017), and Thomas & Pfrommer (2019). Hopkins et al. (2022b) show that this reference model fails to reproduce observed CR spectra and construct an additional "external driving" term, which they show produces good behavior across the diagnostics they consider. This is the transport model adopted here.

The gas and radiation in the simulations not only determine CR transport, but how the CRs act on the resolved fluid. Most importantly, the CRs exert forces on the gas from the Lorentz force and from the CR pressure gradients induced by scattering.

3. Results

3.1. Morphologies

The inclusion of BH feedback affects the morphology of the simulated galaxies. Using the open-source visualization software FIRE Studio (Gurvich 2022), we generated edge-on mock Hubble renderings of the stellar distributions of two Milky Way–mass simulated galaxies, m12q and m12f, and two massive ($>L^*$) galaxies, m13h113 and m13h206, for each of the three models (Figure 1). Milky Way–mass galaxies produce disk-like structures at $z \sim 0$ in simulations without BHs, and in simulations with BHs but no CRs, while the massive galaxies produce a mix of disks and spheroidals for those two models. The addition of CRs in simulations with BHs produces galaxies which appear nearly spherical regardless of mass. The presence of CR feedback in the simulated galaxies produces lower stellar masses (as discussed in Section 3.2) and therefore lower surface brightnesses than in the galaxies without CRs. As the mock images show the stellar content of the galaxies only above a minimum surface brightness, this leads the BH +CR galaxies to appear visually smaller in these images than their counterparts with the same initial conditions, though in fact the BH+CR galaxies are generally physically larger when considering their half-mass radii (as discussed in Section 3.3).

3.2. Masses and Star Formation Rates

Simulations of massive galaxies with AGN feedback can reproduce basic scaling relations at $z \sim 0$. Figure 2 shows how the simulations compare to the stellar mass–halo mass (SMHM) and $M_{\rm BH}$–σ relations at $z \sim 0$. Points are colored by physical model: unfilled black points represent simulations without BHs (the NoBH model), green points represent simulations with BHs but without CRs (the BH model), and purple points represent simulations with both BHs and CR physics (the BH+CR model).

The left panel shows the SMHM relation. Stellar masses for the simulated galaxies are calculated as all stars within $0.1R_{\rm vir}$ of the galaxies' centers, and are compared to the relation presented in Behroozi et al. (2019). At $z \sim 0$, massive galaxies with no AGN feedback have become increasingly overmassive, indicating undersuppressed star formation. By contrast, galaxies with AGN feedback lie much closer to the relation. The two massive galaxies simulated with the BH model lie slightly (around 1σ) above the relation. Massive galaxies with the BH+CR model lie either along the relation or slightly below it; six of the eight galaxies in this subsample are within 1σ, and the remaining two are just below 1σ beneath the relation. The inclusion of CRs as another AGN feedback channel therefore appears to have a significant effect on regulating the stellar mass. However, a few of the Milky Way–mass galaxies with the BH+CR model are significantly undermassive relative to observations, indicating possibly oversuppressed star formation, in contrast to the other two models which more closely reproduce the observed relation at this mass scale. As this model successfully reproduces the SMHM relation for the massive galaxies, this result may suggest that fixed AGN feedback efficiencies like the ones in our model are unable to reproduce the differential quenching at different mass scales implied by observations.

The relationship between stellar mass and stellar velocity dispersion ($M_{\rm BH}$–σ) is another key scaling relation, and both BH models (with and without CRs) reproduce it well. The right panel shows the $M_{\rm BH}$–σ relation for the two models which included BHs, compared to the observational relation from Greene et al. (2020). The stellar velocity dispersion σ is calculated as the standard deviation of the stellar velocities along the stellar angular momentum axis, for stars within the projected half-mass–radius. Almost all of the simulations remain within the intrinsic scatter of the observed relation at $z \sim 0$; only one simulation, an m12 galaxy with the BH model, falls very slightly below it.

In these simulations, BH feedback appears to regulate star formation and self-regulate BH growth. In Figure 3, we examine the star formation histories (SFHs) and BH accretion rates of the four simulated galaxies for which we can compare all three primary models. The SFHs are constructed using an "archeological" method (e.g., as in Flores Velázquez et al. 2021; Gurvich et al. 2023) in which we take all stars within $0.1R_{\rm vir}$ at the final snapshot and estimate their formation masses by accounting for stellar mass loss according to rates from STARBURST99 (Leitherer et al. 1999). We then reconstruct

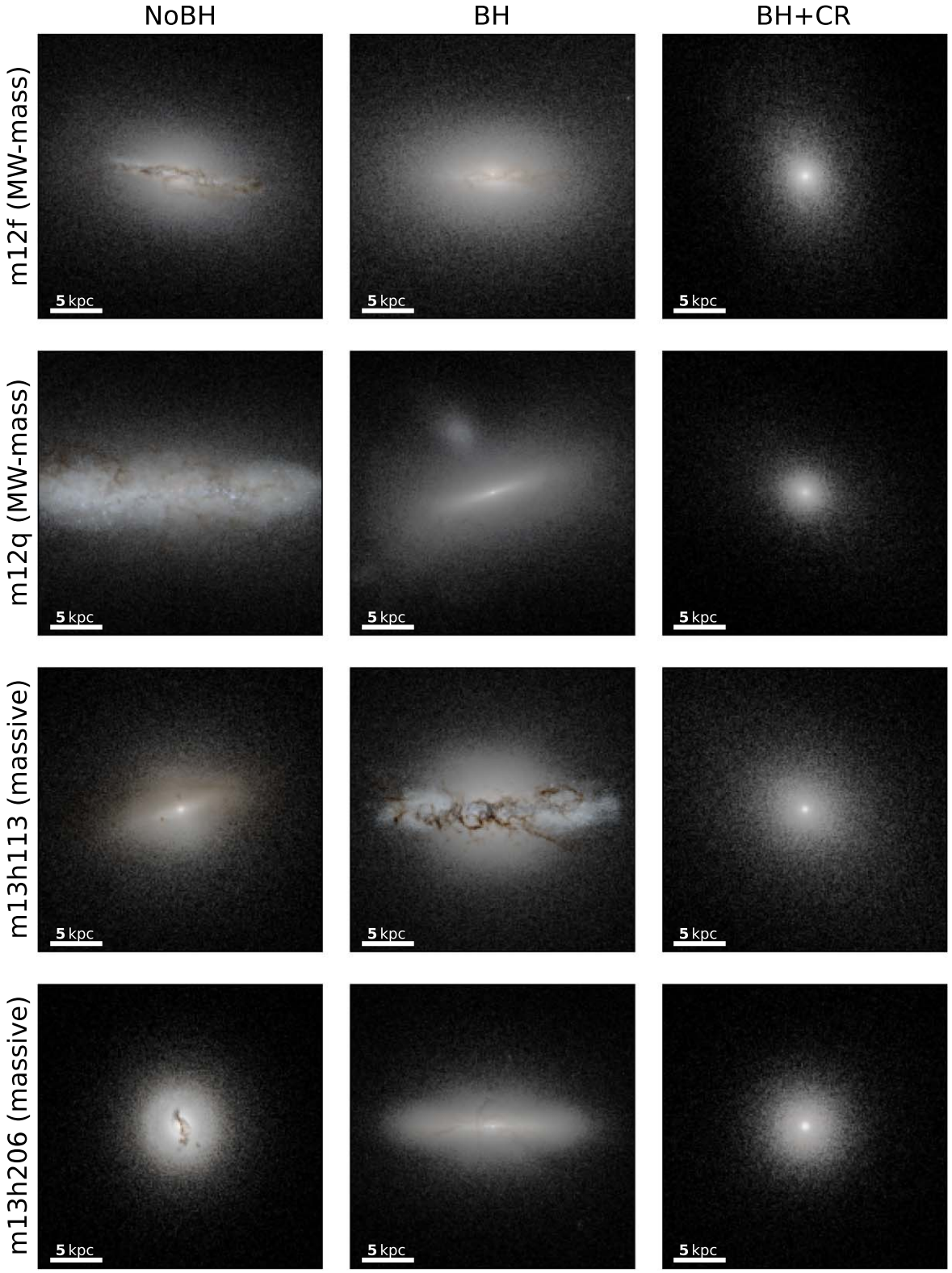

Figure 1. Edge-on mock Hubble images for two example Milky Way–mass simulated galaxies (top two rows) and two example m13 massive galaxies (bottom two rows) at $z \sim 0$. For each set of initial conditions, we compare a model with no BHs or CRs (left) to a model with BHs but no CRs (middle) and to a model with both BHs and CRs (right). Milky Way–mass galaxies tend to be disk-like at $z = 0$ with the NoBH and BH models, while the massive galaxies produce a mix of disks and spheroidals for those two models. The BH+CR model consistently produces elliptical galaxies.

the time-dependent SFHs from the distribution of star particle formation times and star formation masses. Without BH physics included, the SFRs remain steady and relatively constant over the course of the galaxy's lifetime. The inclusion of AGN feedback leads to reductions in the SFRs after a few billion years of the galaxies' lifetimes: Stronger feedback (i.e., the BH+CR model) produces lower SFRs at late times than the BH model, and both produce lower rates than the NoBH model.

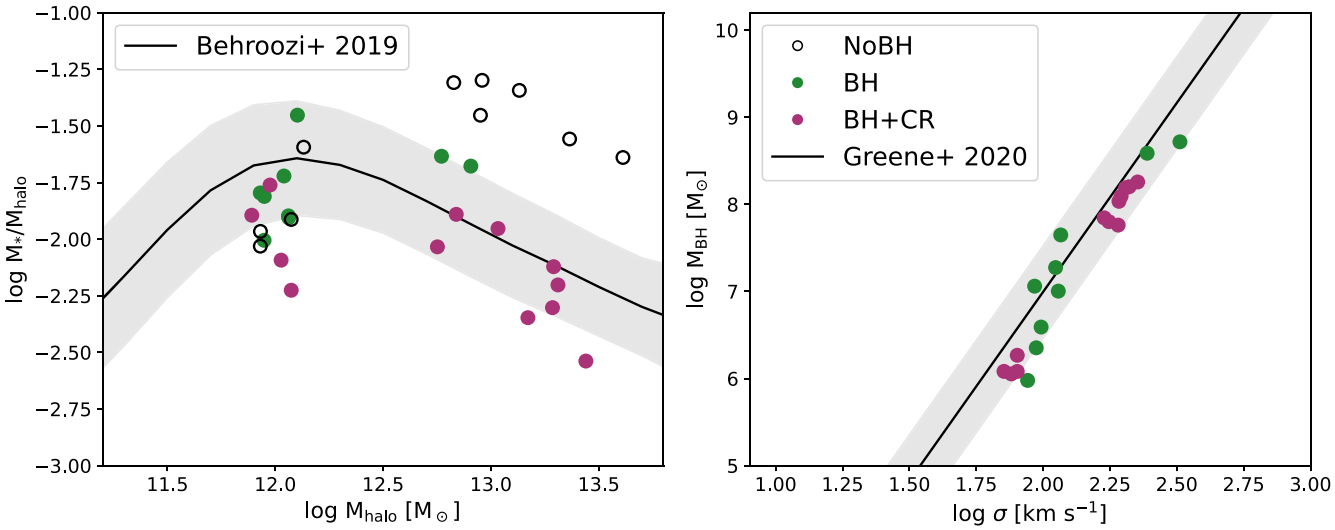

Figure 2. Stellar mass–halo mass (SMHM) relation (left) and $M_{\rm BH}$–σ relation (right) for $z \sim 0$. We compare the NoBH (black, unfilled), BH (green), and BH +CR (purple) models. Left: the SMHM relation from Behroozi et al. (2019) and its intrinsic scatter. Right: the observational $M_{\rm BH}$–σ relation (Greene et al. 2020) and its intrinsic scatter.

The BH accretion rates appear to follow a similar pattern: Stronger feedback in the form of our BH+CR model leads to reduced BH accretion rates, relative to the model without CRs. At times, the BH accretion rates appear to track the SFRs, remaining steady when the star formation is steady, and decreasing at approximately the same time as major star formation quenching episodes. While not every feature of the SFHs appears in the BH accretion histories, this general correlation is indicative that both stars and BHs in the galactic nuclei are drawing on a common gas supply—and BH feedback reducing that gas supply can regulate both star formation and the growth of the BH itself.

Figure 4 shows the specific SFR for each simulation at $z \sim 0$, averaged over 10 Myr, along with observed specific SFRs for the star-forming sequence from Salim et al. (2007). We indicate the stellar mass at which 50% of galaxies are expected to be quenched at $z = 0$ (Behroozi et al. 2019), along with the interquartile range of the quenched fraction from 25% to 75%. Contrary to observations, the stronger feedback model (BH +CR) appears to quench all Milky Way–mass m12 galaxies. The BH and NoBH models produce a more realistic mixture of star-forming and quenched galaxies at this mass scale.

For massive galaxies, however, observations do indicate a substantial population of quenched galaxies, and the BH+CR model is the only model to fulfill this requirement. SFRs for massive m13 galaxies with no AGN feedback remain at or above the star-forming sequence. Similarly, neither of the two massive galaxies produced with the BH model are quiescent. By contrast, all galaxies evolved with the BH+CR model are well below the star-forming sequences, indicating that strong feedback, such as the additional energy from CRs in this model, is necessary to produce a quiescent population of massive galaxies. Many of these massive galaxies with AGN feedback and CRs are quenched entirely, while a few retain small amounts of star formation, consistent with observations.

3.3. Structural Properties

Simulations without AGN have struggled to produce realistic galaxy sizes at the massive end, as without AGN feedback massive galaxies can become overly compact by an order of magnitude (e.g., Choi et al. 2017, 2018; Wellons et al. 2020; Parsotan et al. 2021; Cochrane et al. 2023). We consider the impact of AGN feedback on galaxy sizes in our simulations. Figure 5 shows the relationship between the stellar mass and the stellar half-mass–radius, which is calculated as the radius at which the cumulative stellar mass profile reaches half the total stellar mass, taking the average after projecting along five randomly selected angles. Galaxy sizes are compared to the observational R_e–M_* relations found by Baldry et al. (2012), assuming a constant mass-to-light ratio, which is a reasonable approximation for old stellar populations. Simulated massive galaxies without AGN feedback (the NoBH model) are too compact by an order of magnitude; given their high stellar masses, this indicates that these galaxies are dramatically more compact than observed galaxies. By contrast, simulations with the BH+CR model are almost all consistent with observations: All four m12s, and seven out of eight m13s, are within the scatter of the observed relation. The BH+CR model performs better by this metric than the BH model, as several m12 galaxies and both m13 galaxies with the latter model are also overly compact relative to observations.

This further indicates that strong AGN feedback is necessary to produce realistic massive galaxies; without the additional energy from CRs, the BH model we analyze cannot prevent overcooling or produce realistic galaxy sizes. To disentangle the effects of stellar versus AGN CRs, we include in Figure 5 two simulations with stellar CRs but no AGN feedback (NoBH +CR): an m12 galaxy with $M_* \approx 10^{10.5}\,M_\odot$ and an m13 galaxy with $M_* \approx 10^{11.4}\,M_\odot$, shown in the figure as blue diamonds. The size of the NoBH+CR m12 galaxy is close to but slightly below the observed relation, similar to several of the BH +CR m12 galaxies. The m13 massive galaxy with the NoBH +CR model, meanwhile, is overly compact by more than an order of magnitude and not physically realistic by $z = 0.5$. This run failed catastrophically and unrecoverably at this early redshift due to the computational expense of the CR model when combined with an unphysically dense stellar core. We conclude that the inclusion of stellar CRs alone, i.e., without AGN feedback, does not produce realistic galaxies at the

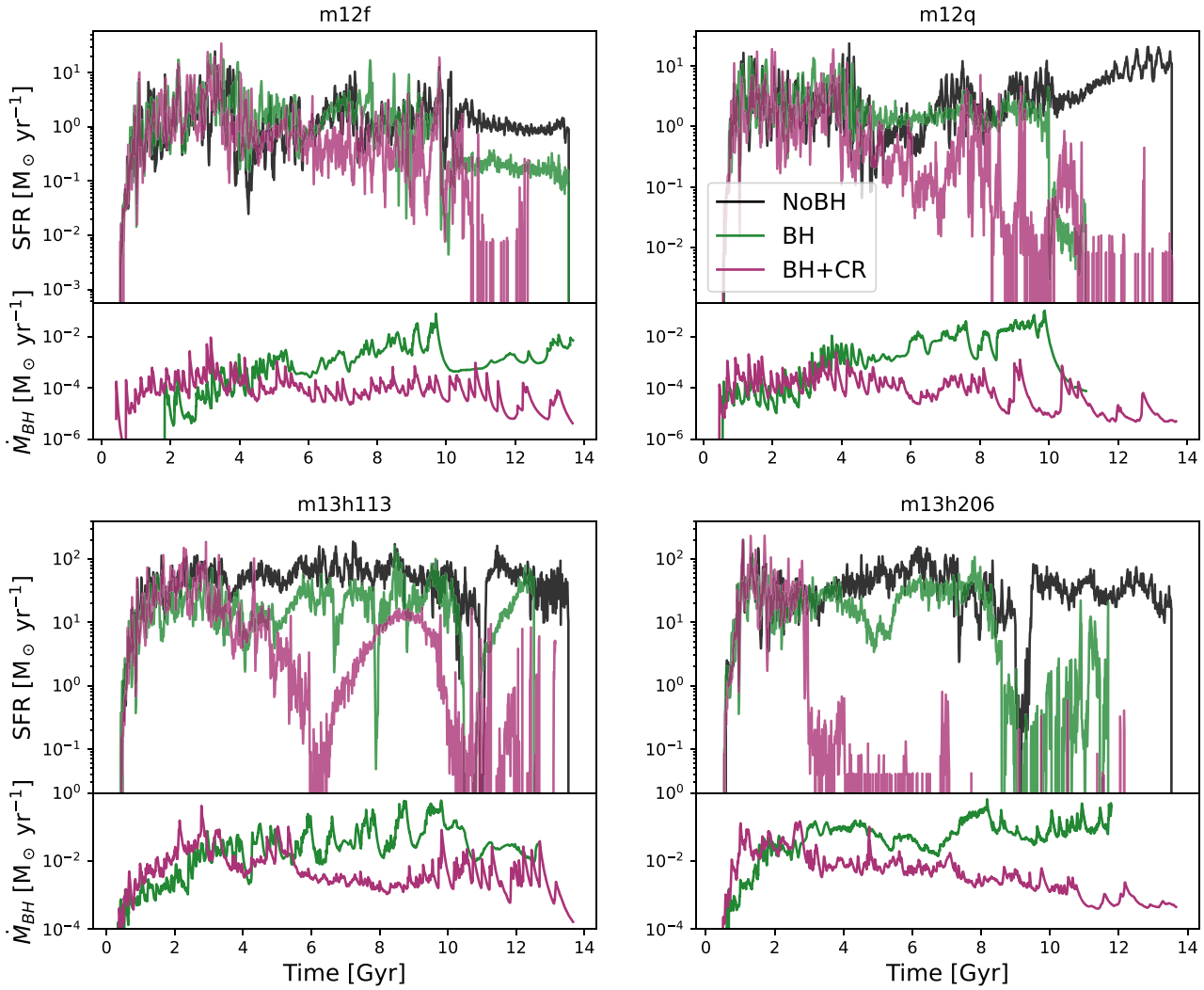

Figure 3. Star formation histories and BH accretion histories for the same four example simulated galaxies shown in Figure 1: two Milky Way–mass galaxies (upper) and two massive galaxies (lower). We compare three different physics models: NoBH (black), BH (green), and BH+CR (purple). The inclusion of BH feedback reduces the SFR at later times compared to the SFRs in simulations without BH feedback. This effect is particularly strong for the BH+CR model in simulations of massive (m13) galaxies, in which the SFR is consistently lower than for the other models starting early in the galaxies' lifetimes. In addition to having lower SFRs than the BH model, the BH+CR model also produces lower BH accretion rates.

massive end but may produce reasonable properties at the $\sim L^*$ mass scale.

Another important scaling relation is the relationship between stellar velocity dispersion σ and stellar mass—the Faber–Jackson relation (Faber & Jackson 1976). Figure 6 shows this relation for all simulations at $z \sim 0$. While all but a few of the simulated Milky Way–mass m12 galaxies, both with and without AGN feedback, fall within the intrinsic scatter of the observed relation found by Gallazzi et al. (2006), the inclusion of AGN feedback appears to have a profound impact on massive galaxies. All but one of the simulated massive galaxies without AGN feedback have overly high velocity dispersions, 0.3–0.5 dex above the intrinsic scatter of the observations. By contrast, simulated massive galaxies with the BH+CR model lie on or near the relation, and massive galaxies with the BH model lie slightly (within <0.2 dex) above it. The inclusion of BH feedback therefore appears to be key to successfully reproducing this relation for massive galaxies: The lower stellar masses and larger sizes of the galaxies with BH feedback reduce the velocity dispersions to more realistic levels, since $\sigma \propto \sqrt{M/R}$. As in Figure 5, we analyze the effects of stellar CRs by including two simulations with stellar CRs but no AGN feedback, plotted as blue diamonds. The m12 galaxy with the NoBH+CR model lies along the observed relation. The m13 NoBH+CR galaxy has an unrealistically high stellar velocity dispersion, similar to the NoBH galaxies. The failure of the massive galaxy with the NoBH+CR model is a further indication that AGN feedback, not stellar CRs, is responsible for producing realistic galaxies at this mass scale, in agreement with Figure 5.

In Figure 7, we examine the stellar surface density profiles for the massive galaxies in our simulated sample. Projected stellar surface densities are calculated in radial annuli and shown as a function of $r^{1/4}$ (de Vaucouleurs 1948). Observed profiles of local massive ellipticals (gray) are reproduced from Hopkins et al. (2010), where observations from Lauer et al. (2007) are separated into "cusp" and "core" systems with average stellar masses $M_* = 10^{10.8}\,M_\odot$ and $M_* = 10^{11.6}\,M_\odot$, respectively. Simulations with the BH+CR model are comparable in mass to the cusp systems, while the NoBH galaxies are comparable to the core systems, and the galaxies with the BH model span the mass range between cusp and core. All

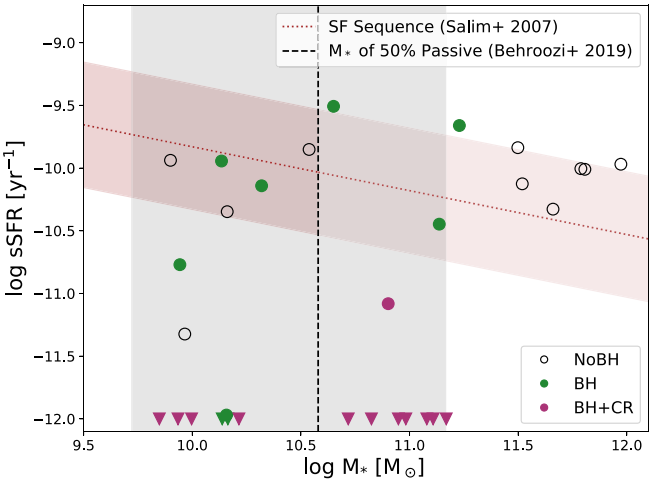

Figure 4. Specific SFR vs. stellar mass of the galaxy at $z \sim 0$. We compare the NoBH (black, unfilled), BH (green), and BH+CR (purple) models. Triangles indicate upper limits. Observed specific SFRs from Salim et al. (2007) are shown for the star-forming sequence (dotted red line) along with the intrinsic observed scatter (red shaded region). We indicate the stellar mass at which 50% of galaxies are expected to be quenched with a black dashed line (Behroozi et al. 2019); the gray shaded region represents the interquartile range of the quenched fraction from 25% to 75%. The NoBH model produces galaxies which are consistently star-forming, while the BH+CR model produces galaxies that are consistently quenched. The BH model produces a mixture of quenched and star-forming Milky Way–mass galaxies; however, neither of the two most massive galaxies evolved with this model were quenched.

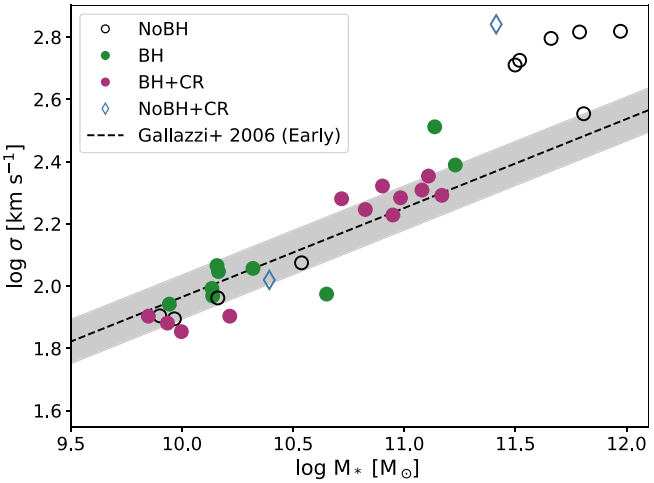

Figure 6. Stellar velocity dispersion vs. stellar mass for galaxies at redshift $z \sim 0$, compared to the observed relation for early-type galaxies found by Gallazzi et al. (2006). We compare the NoBH (black, unfilled), BH (green), and BH+CR (purple) models, as well as two galaxies with the NoBH +CR model (open blue diamonds). At the massive end, the NoBH and NoBH +CR simulations have clearly too high velocity dispersions, while massive galaxies with the BH+CR model lie on or near the observed relation, and massive galaxies with the BH model lie slightly above it. For Milky Way–mass galaxies, all galaxies produced with the NoBH model and all but one with the BH model lie near the relation, while two of the four galaxies with the BH +CR model lie slightly below it. Overall, these results show that strong AGN feedback is needed to reproduce observed velocity dispersions at the massive end, and that CRs from stars alone are not sufficient.

simulated galaxies with AGN feedback produce stellar profiles

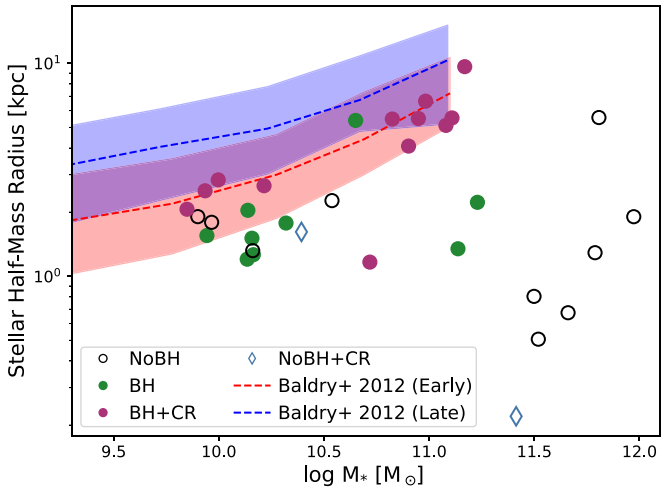

Figure 5. Projected stellar half-mass–radius vs. stellar mass for galaxies at redshift $z \sim 0$, compared to the observations of projected half-light radii from Baldry et al. (2012). The red observational band corresponds to early-type galaxies and the blue band to late-type galaxies. We compare the NoBH (black, unfilled), BH (green), and BH+CR (purple) models, as well as two galaxies with the NoBH+CR model (open blue diamonds). Massive galaxies with the NoBH model are consistently order-of-magnitude overly compact, while all but one of the simulations with the BH+CR model are consistent with observed early-type galaxies. Massive galaxies with the BH model, without CRs, tend to be overly compact but not to the same degree as the NoBH galaxies. The open diamond at $M_* \approx 10^{11.4}\,M_\odot$ shows that a massive galaxy evolved to $z = 0.5$ including stellar CRs but no AGN feedback (the NoBH+CR model) is an order of magnitude too compact, similar to the NoBH model and indicating that stellar CRs are not sufficient to explain stellar sizes at the massive end.

outside of 1 kpc which are in good agreement with observations. Simulations without BH feedback are overdense by up to 2 orders of magnitude in the inner regions, while simulations with BH feedback but no CRs are overdense by up to 1 order of magnitude. Introducing BH feedback with CRs reduces stellar densities to more realistic levels, though they are still too high by a factor of a few in the central regions.

For context, we also compare our density profiles to profiles of massive galaxies from other cosmological simulations with AGN feedback included: the average of IllustrisTNG early-type galaxies with $10^{10.5}\,M_\odot < M_* < 10^{11}\,M_\odot$ (Cannarozzo et al. 2023), an early-type EAGLE galaxy (Rosito et al. 2019), three massive Magneticum galaxies (one brightest cluster galaxy and two other early-type galaxies, selected to match in stellar mass three observed galaxies with different radial profiles: A1400 BCG, NGC 3379, and NGC 2284; Remus & Forbes 2022), and a $M_* = 3.2 \times 10^{11}\,M_\odot$ elliptical galaxy studied in Dubois et al. (2013).[11] Different models with AGN feedback, including ours, do comparably well at reproducing the stellar density profiles outside ~1 kpc. The high resolution of our simulations allows us to plot predicted stellar densities down to small projected radii: The stellar softening lengths for massive galaxies in our simulations are $\epsilon_{\rm star} = 8$–18 pc, while the resolutions for the comparison simulations are $\epsilon_{\rm star} = 740$ pc for IllustrisTNG, $\epsilon_{\rm star} = 700$ pc for EAGLE (Schaye et al. 2015), $\epsilon_{\rm star} = 700$ pc for Magneticum, and a minimum cell size $\Delta x = 500$ pc for Dubois et al. (2013). Within a radius $r < 1$ kpc, our simulations predict significantly higher stellar densities than the observations compiled. This is a potentially significant discrepancy that our zoom-in simulations allow us to identify in a regime which could not be tested in lower-resolution simulations.

While the BH+CR runs are overall the best match to the observed stellar profiles, Figure 7 suggests that these runs predict stellar "cores" with a significant change of slope at

[11] The surface density profile for this galaxy was inferred from the published data by integrating the three-dimensional density profile along the line of sight, assuming spherical symmetry.

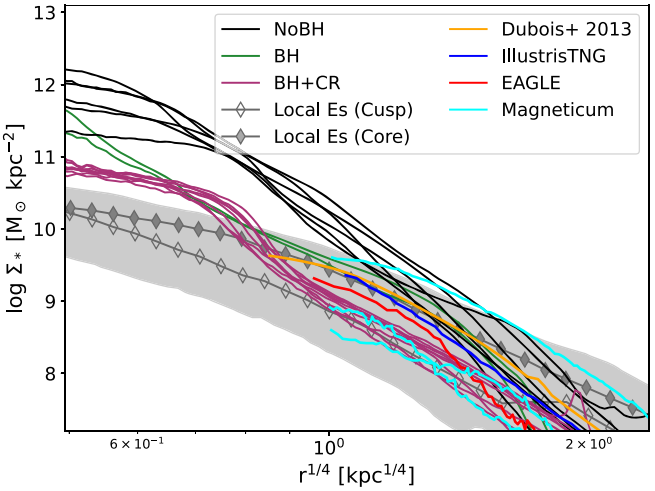

Figure 7. Stellar surface density profiles for massive galaxies with the NoBH (black, unfilled), BH (green), and BH+CR (purple) models. Stellar surface densities are calculated in radial annuli and shown as a function of $r^{1/4}$. Observed profiles of local massive ellipticals (gray) are reproduced from Hopkins et al. (2010), with observations from Lauer et al. (2007) separated into "cusp" and "core" systems. The shaded regions represent the 1σ scatter for the observed sample. The profiles of massive, early-type galaxies from other cosmological simulations with AGN feedback are also included from Dubois et al. (2013), EAGLE (Rosito et al. 2019), IllustrisTNG (Cannarozzo et al. 2023), and Magneticum (Remus & Forbes 2022). The NoBH galaxies are comparable in total stellar mass to the observed "core" galaxies (average $M_* = 10^{11.6}\,M_\odot$), while the BH+CR galaxies are comparable in mass to the "cusp" galaxies (average $M_* = 10^{10.8}\,M_\odot$), and the BH galaxies lie somewhere in between. Simulations without BH feedback are overdense by up to 2 orders of magnitude in the inner regions. Introducing BH feedback reduces stellar densities: Galaxies with BH feedback are overly dense in the central regions, but converge to observations by 1 kpc; with CRs included in addition, the central stellar surface densities are further reduced, though still too high in the innermost regions.

$r \sim 0.4$ kpc ($r^{1/4} \sim 0.8$ kpc$^{1/4}$). The relatively abrupt change in slope is unusual for stellar profiles, but it is on a scale substantially larger than the gravitational softening for stars in those runs ($\epsilon_{\rm star} = 18$ pc). Moreover, the cores are resolved by well over 10^4 stellar particles and have masses $\gtrsim$10$\times$ the masses of the central BHs. We also note that the NoBH runs in the figure were run with the same resolution and do not show signs of unphysical features in their stellar profiles. Therefore, the inner stellar profiles in the BH+CR runs may be the result of complex interactions involving the baryonic processes, including the CR physics, which would be interesting to investigate more in future work.

We examine the effects of AGN feedback on the kinematic characteristics of each galaxy in Figure 8, which shows the the mass-weighted normalized distributions of the orbital circularity ϵ of every star particle within $0.1R_{\rm vir}$ in each galaxy. Circularity $\epsilon = j_z/j_c(E)$ is defined as the ratio of each particle's angular momentum in the $\hat{z}$ direction to that of a circular orbit with the same energy (Abadi et al. 2002). Following Scannapieco et al. (2008), we define $j_c(E) = rv_c = r\sqrt{GM_{\rm enc}/r}$ for a particle at radius r, a reasonable approximation for galaxies with spherically symmetric potentials. A spheroidal galaxy will have a circularity distribution centered around $\epsilon = 0$, while for a rotation-supported disk the distribution will peak at $\epsilon = 1$. Galaxies with both a disk and a bulge will have multiple peaks. We find that simulations without BHs, or with BHs but no CRs, tend to produce a mixture of morphologies, including many galaxies with a significant disk component. The BH+CR model, however, is unable to produce a realistic population of disk galaxies at $\sim L^*$, providing further evidence that the feedback in this model may be too strong at that mass scale. This model consistently produces spheroidal galaxies with distributions peaking at $\epsilon = 0$, as is also visually suggested in Figure 1.

4. Discussion

4.1. Scaling Relations and the Quenching of Star Formation

We demonstrate that cosmological simulations with detailed stellar and ISM physics combined with multichannel AGN feedback can successfully produce massive galaxies with little or no star formation, broadly in agreement to observations which show galaxy populations dominated by quenched galaxies at stellar masses of $M_* \gtrsim 10^{10.5}\,M_\odot$. This is in contrast to simulations without AGN feedback which generally do not quench, especially at the massive end (the m13 galaxies in our study; see Figures 3 and 4). This provides evidence that BH feedback is necessary to produce a realistic bimodal population of galaxies. The reduction in star formation for galaxies at the massive end when AGN feedback is included is in broad agreement with many simulations using other codes (e.g., Di Matteo et al. 2005; Dubois et al. 2012; Schaye et al. 2015; Weinberger et al. 2017, 2018, 2023).

While it has been shown in many previous simulations that AGN feedback can produce massive galaxies with broadly realistic properties, our results are significant because none of the previously published FIRE cosmological zoom-in simulations, which include detailed stellar feedback physics, produced any quenched galaxies with realistic properties at the massive end (e.g., Hopkins et al. 2014, 2018, 2023; Wellons et al. 2020). This was the case even when exploring the impact of various "extra physics" other than AGN feedback, including magnetic fields and CRs from stellar processes (e.g., Hopkins et al. 2020a). The earlier FIRE study by Wellons et al. (2023) first analyzed a suite of FIRE-2 cosmological simulations including AGN feedback and showed preliminary successes, but the present study based on the FIRE-3 code presents a much more detailed comparison to different observational metrics.

Beyond quenching star formation, we show that simulations of massive galaxies with AGN feedback can successfully match local scaling relations including the SMHM relation (Figure 2, left), the $M_{\rm BH}$–σ relation (Figure 2, right), the size–mass relation (Figure 5), and the Faber–Jackson relation (M_*–σ, Figure 6). Previous FIRE simulations demonstrated that in the absence of AGN feedback, massive galaxies generically become too compact and overly dense, falling well below the observed size–mass relation (Wellons et al. 2020; Parsotan et al. 2021). Our results (see Figures 5 and 7) show, in agreement with some previous work, that the inclusion of AGN feedback can increase the size of massive galaxies and reduce their central stellar densities, producing much more realistic galaxy sizes (Dubois et al. 2016; Choi et al. 2018; Cochrane et al. 2023).

As we discuss further in Section 4.3 below, our results are best viewed as a demonstration that some choices of AGN feedback parameters produce broadly realistic, quenched, elliptical galaxies at the massive end in the FIRE simulation framework. However, this is certainly not the final word on AGN feedback as we find evidence that fixed AGN parameters

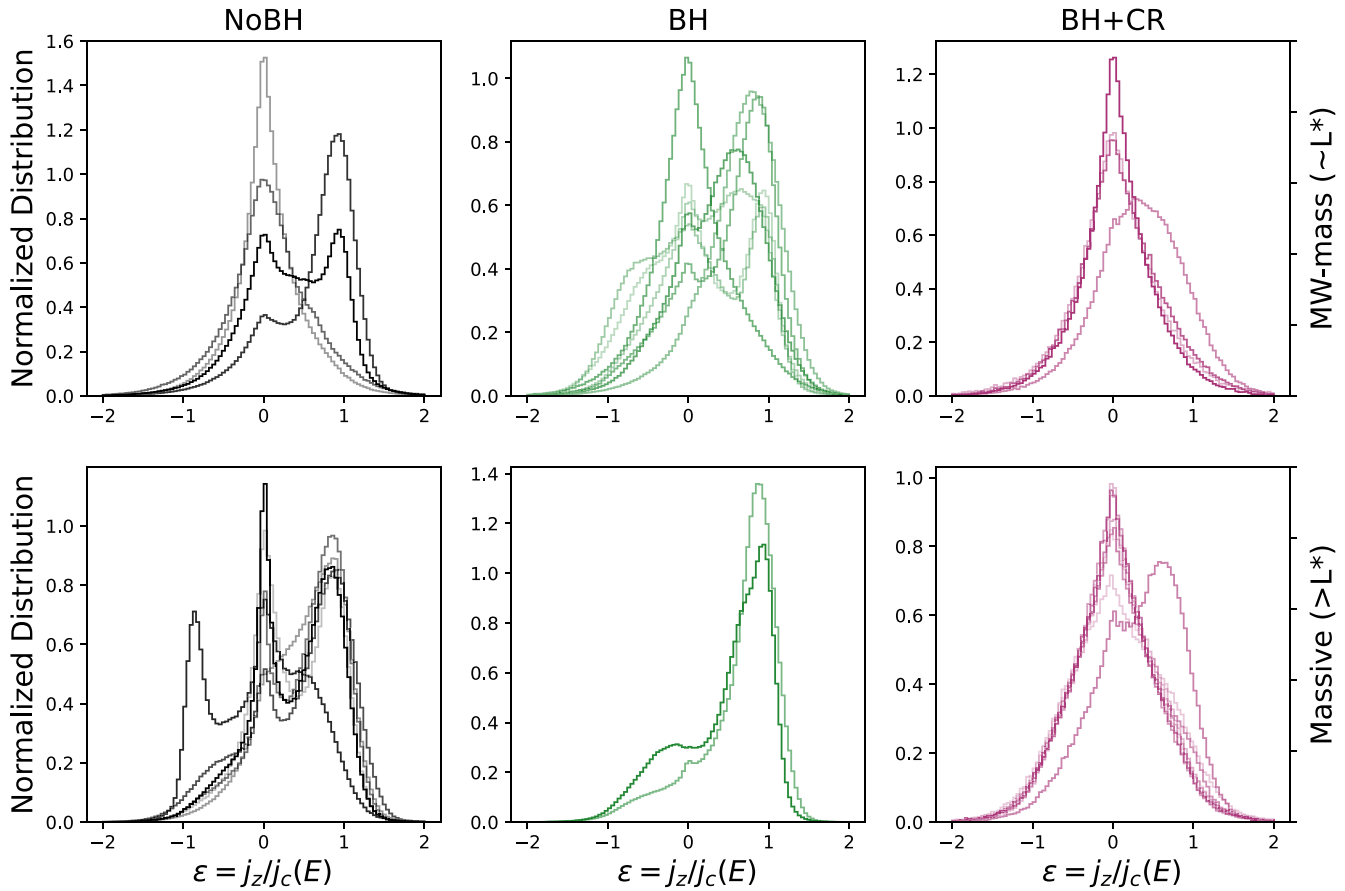

Figure 8. Mass-weighted normalized distributions of the circularity parameter $\epsilon = j_z/j_c(E)$ of star particles in each simulation. Each line represents an individual simulation. Histograms are categorized by mass scale, Milky Way–mass m12s (top) and massive m13s (bottom), and by model, NoBH (left), BH (center), and BH +CR (right). Distributions with peaks around $\epsilon = 0$ indicate elliptical morphologies, while peaks at $\epsilon = 1$ indicate disk-like morphologies.

do not produce uniformly realistic galaxies at all mass scales—perhaps indicating a mass dependence of AGN feedback physics.

4.2. The Role of Cosmic Rays

We find that our model of AGN feedback including CRs is more efficient at quenching star formation than the AGN feedback model with only radiative and kinetic feedback channels. In the simulations presented in this paper, while both BH feedback models produce massive galaxies which better match observed properties than the model without BHs, we found that the BH+CR model was more successful at reproducing the size–mass and M_*–σ relations (Figures 5 and 6) than the BH model, which produced massive galaxies that were unrealistically compact and with too-high velocity dispersions. Galaxies simulated with the BH+CR model also display more drastic reductions in their SFRs than galaxies simulated with the BH model. Neither of the two massive galaxies evolved with this model became quiescent. However, the BH+CR model in some ways appears to be too strong: It overquenches Milky Way–mass galaxies, and consistently produces nearly spherical ellipticals across the mass range studied in this paper (Figures 1 and 4). The lack of any disk-like galaxies produced with this model, even at the Milky Way–mass scale, shows that this model has shortcomings. It is important to note that substantial uncertainty remains as to how best to model CR transport. Exploring the effect of alternate CR models, and improving this model to produce a more realistically diverse population of galaxies at different mass scales, will be critical for future work.

Overall, our results are consistent with previous studies using FIRE simulations which found that AGN feedback in the form of CRs could have a significant impact on galaxy quenching. Wellons et al. (2023) found that the inclusion of CRs significantly increases the potential of a BH to suppress star formation even when the energy in CRs is relatively low. In simulations using the FIRE physics but of isolated halos (without the cosmological environment) in the mass range $M_{\rm halo} \sim 10^{12}$–$10^{14}\,M_\odot$, Su et al. (2020) found that CR jets suppress cooling flows more effectively than thermal heating or momentum injection, while Su et al. (2021) found that CR-dominated jets are able to quench galaxies with order-of-magnitude lower energetics than jets dominated by thermal or kinetic energy (see also Su et al. 2024). It is worth noting, however, that the simulations in those works used a CR model with constant diffusion, while we use a model in which CR transport depends on local plasma properties (see Section 2.2). In the set of simulations used in this work, CR pressure is subdominant in the CGM (I. Sultan et al. 2024, in preparation), in contrast to constant diffusion models which can produce CGMs dominated by CRs at the L^* mass scale (e.g., Ji et al. 2020, 2021; Butsky et al. 2023).

As the BH+CR model includes CRs from both stellar and BH feedback, it is useful to determine whether these differences are driven by BH feedback or if stellar CRs could be the cause. Fully disentangling the effects of stellar CRs from

BH+CR feedback is beyond the scope of this work, but we comment here on what we can infer from previous work and the runs in this paper. In this paper, we tested a fourth physics model with CRs from stellar feedback processes but without BHs (the "NoBH+CR" model) on one FIRE-3 m12 and one m13 galaxy (see Table 2). The m12 galaxy was integrated down to a redshift of $z = 0$, while the simulation of the m13 galaxy with the NoBH+CR model failed at $z = 0.5$ after it became overly compact (see Figure 5). While the m12 galaxy with the NoBH+CR model produced generally realistic results, the m13 galaxy with the NoBH+CR model showed similar properties as the m13 galaxies with the NoBH model: It failed to reproduce the observed SMHM, size–mass, and M_*–σ relations due to being overmassive, too compact, and having overly high stellar velocity dispersions. It also was continuously star-forming until the final snapshot at $z = 0.5$, several billion years after all simulations with the BH +CR model had already quenched. For these reasons, the success of the BH+CR model at the massive end appears to rely crucially on CRs from BH feedback, not CRs from stellar sources.

It is worth noting that the total amounts of CR energy from stellar feedback and BH feedback are comparable in the simulations when integrated over the age of the universe. To see this, note that there is about one supernova per $100\,M_\odot$ of stars formed, so the integrated energy in CRs from stars is $E_{\rm CR}^{\star} \approx 0.1 \times 10^{51}\,{\rm erg}\,(M_\star/100\,M_\odot) = 10^{59}\ M_{\star,11}$ erg, where $M_{\star,11} \equiv M_\star/10^{11}\,M_\odot$. Similarly, the integrated energy in CRs from the BH is $E_{\rm CR}^{\rm BH} = \epsilon_{\rm CR}^{\rm BH} M_{\rm BH} c^2 \approx 1.8 \times 10^{59}\,{\rm erg}\,M_{\rm BH,8}\epsilon_{\rm CR,-3}^{\rm BH}$, where $M_{\rm BH,8} \equiv M_{\rm BH}/10^8\,M_\odot$ and $\epsilon_{\rm CR,-3}^{\rm BH} \equiv \epsilon_{\rm CR}^{\rm BH}/10^{-3}$. This suggests that total feedback energy alone does not determine the impact on a galaxy's star formation. The lack of a CR-dominated halo for these simulations (Sultan et al. 2024, in preparation) indicates that our CR transport model produces high-energy CR outbursts which can escape from the halo, rather than the smooth CR injection into the halo seen in simulations with a constant diffusion model. These results are therefore consistent with the findings of Wellons et al. (2023), who found that the responsiveness of the AGN feedback model—that is, how quickly and powerfully the BH will respond to changes in its environment, for example by creating bursts of feedback when gas in the accretion kernel is abundant—plays an important role in determining whether galaxies quench. This suggests that CRs from AGN feedback may be more efficient at suppressing star formation than CRs from stellar feedback because the AGN duty cycle produces strong outbursts of CRs, while the CR injection from stellar sources is more time steady on average.

The successes of the BH+CR model demonstrate that multichannel AGN feedback can resolve some of the main failures of simulations without SMBHs in FIRE simulations with resolved ISM physics. However, we emphasize that this study analyzed only two fixed AGN feedback variants. In particular, we cannot conclude that CRs are the only way of achieving the successes we found in the BH+CR runs. It is possible, for instance, that the BH+CR model is best viewed as a "stronger" AGN feedback model than the specific BH model we analyzed. In a broader survey of AGN feedback parameters using FIRE-2 test simulations, Wellons et al. (2023) showed that while CRs from AGN feedback can efficiently quench galaxies, feedback variants in which the kinetic wind efficiency is increased can also quench massive galaxies. We therefore stress that further work will be needed to fully disentangle the roles of different feedback processes, including CRs.

4.3. Evidence for a Mass Dependence of Active Galactic Nuclei Feedback

In the simulations presented in this paper, the frequency with which galaxies quenched is plausibly realistic for massive galaxies but perhaps too high for Milky Way–mass galaxies (Figure 4). The reduced star formation in Milky Way–mass galaxies leads to final stellar masses which are in some cases significantly below the observed SMHM relation. These results are broadly consistent with other studies of both hydrodynamic and semi-analytic models which have found that it is necessary for AGN feedback to become more efficient above a critical mass scale of $\sim L^*$ for simulations to reproduce the observed bimodality (e.g., Croton et al. 2006; Nelson et al. 2018).

Rather than enforcing an explicit mass scale for AGN activity or star formation quenching, we chose to use fixed AGN feedback efficiencies. Our simulations capture the multiphase ISM and CGM at high resolution, and self-consistently resolve the formation of hot halos and the transition from bursty to steady star formation, both of which appear to occur at approximately the same galaxy mass as the critical mass scale for AGN feedback (Anglés-Alcázar et al. 2017b; Bower et al. 2017; Habouzit et al. 2017; Stern et al. 2021; Byrne et al. 2023). The lack of an explicitly set mass scale in our models allows us to investigate whether the mass scales set by these processes alone could be responsible for the transition from inefficient to efficient AGN feedback. Our findings suggest that this is not the case: Resolving these processes self-consistently does not appear to be sufficient to produce the critical mass scale above which AGN feedback is effective at quenching star formation, and below which it is not.

However, the subgrid treatment of BH accretion remains a source of uncertainty, with only recent cosmological hyper-refinement simulations able to explicitly model gas inflow rates down to scales <0.1 pc (Anglés-Alcázar et al. 2021). In addition, our BH-feedback model is mass invariant, in the sense that energy proportional to accretion rate is being injected independently of the Eddington ratio, the spin of the BH, the magnetic field properties, etc. We have not yet determined to what extent these types of small-scale accretion-flow physics may affect the large-scale properties of AGN feedback in our simulations. In future work, we plan to update the accretion model to incorporate insights from smaller-scale simulations about these physical processes.

5. Summary and Conclusions

We present the first set of FIRE-3 simulations of massive galaxies evolved with multichannel AGN feedback. These high-resolution, cosmological zoom-in simulations combine detailed stellar physics and a resolved multiphase ISM with multichannel AGN feedback in the forms of radiative feedback, mechanical outflows, and CRs. The combination of a highly resolved ISM with detailed multichannel stellar and AGN feedback processes distinguishes this work from existing large-volume cosmological simulations.

We simulate galaxies with halos in the mass range 10^{12}–$10^{13}\,M_\odot$ down to low redshift. While no previous FIRE simulations including detailed stellar physics but neglecting BHs succeeded in producing realistic galaxies at the massive

end of this halo mass range, we demonstrate that the addition of AGN feedback produces much improved and broadly realistic galaxy properties in several example runs of $>L^*$ galaxies evolved to $z \sim 0$.

We test two AGN feedback models: the BH model, which includes both radiative and kinetic feedback channels, and the BH+CR model, which additionally includes feedback in the form of CRs. These models are both more successful at reproducing observations of massive galaxies than simulations without AGN (the NoBH model), which can fail to match observed properties such as galaxy sizes by an order of magnitude. However, the analysis reveals some limitations of the AGN feedback models: Without CRs, the massive galaxies do not match all scaling relations, while the inclusion of CRs produces galaxies that are consistently quenched and spheroidal even at the lower, $\sim L^*$ mass scales where observations indicate that a large fraction of all galaxies are still star-forming and disky.

Our main specific results are as follows:

1. The addition of BH feedback affects the morphology of the galaxies. For the same set of initial conditions, a galaxy that looks like a disk in the absence of BH feedback can become spheroidal when feedback is included. Strong feedback, such as in our BH +CR model, appears to consistently produce spheroidal galaxies, while the weaker BH feedback model produced a mixture of disk and spheroidal galaxies. We demonstrate this through both visual inspection of the stellar distributions and by examining the distributions of the orbital circularities of star particles.
2. Massive galaxies simulated with either the BH or the BH +CR model can reproduce several observed low-redshift scaling relations, including the observed SMHM and $M_{\rm BH}$–σ relations. Without AGN feedback, simulated galaxies have stellar masses which are consistently too high relative to their halo masses by a factor of 3–5.
3. The presence of AGN feedback can quench star formation in massive galaxies. Massive galaxies in simulations without BH physics consistently remain actively star-forming regardless of their mass: Their SFRs are roughly constant throughout their lifetimes, and their specific SFRs remain at or above the star-forming sequence as of $z \sim 0$. By contrast, many simulations including BH feedback produce quenched galaxies. Comparing the SFHs of galaxies with the same initial conditions evolved with each of our models, we find that the inclusion of AGN feedback leads to reductions in the SFRs after a few billion years of the galaxies' lifetimes: Stronger feedback (i.e., the BH+CR model) produces lower SFRs at late times than the BH model, and both produce lower rates than the NoBH model. By redshift $z \sim 0$, most massive galaxies with BH+CR model AGN feedback are quenched.
4. AGN feedback also produces galaxies with more realistic structural properties. We demonstrate that our stronger AGN feedback model, which includes CRs, generally increases galaxy half-mass radii to be consistent with the observed size–mass relation, reduce stellar velocity dispersions to levels broadly consistent with observations of the Faber–Jackson (M_*–σ) relation, and reduce stellar surface densities in the central regions of the galaxies. By contrast, simulations without AGN feedback produce galaxies inconsistent with observed properties by up to an order of magnitude. The weaker BH model without CRs is less successful at reproducing some of these relations for massive galaxies than the BH+CR model, though it still represents a significant improvement relative to the model with no BHs at all.

There are several interesting directions for future work. First, it will be necessary to continue improving our AGN feedback model in order to create a model which can produce realistic galaxies across all galaxy masses, which neither of our models currently achieve. The BH accretion and feedback models used in this work are mass invariant, and our results suggest that these models do not accurately capture the differential quenching rates for galaxies at different mass scales, even with a highly resolved ISM and self-consistently resolved hot halo formation and star formation burstiness. In future work, we plan to explore additional physics that could potentially introduce a mass dependence on the global effect of AGN feedback. For example, the Eddington ratio, BH spin, or magnetic flux could affect the accretion disk properties and therefore the intrinsic AGN feedback efficiencies, and we plan to investigate these effects. Additionally, we do not yet fully understand how each separate AGN feedback channel (radiation, winds, or CRs) acts upon the galaxies and their environments, so further analysis of the effects of these individual channels will be critical. As the sample size of simulations studied in this work is relatively small, a future analysis involving a larger sample and more parameter variations would help both in disentangling the effects of different feedback mechanisms and allow for a more statistically rigorous comparisons to observations.

Acknowledgments

We thank the referee for comments that helped us clarify this paper. L.B. was supported by the DOE Computer Science Graduate Fellowship through grant No. DE-SC0020347. C.A. F.G. was supported by the NSF through grants AST-2108230, AST-2307327, and CAREER award AST-1652522; by NASA through grant Nos. 17-ATP17-0067 and 21-ATP21-0036; by STScI through grant No. HST-GO-16730.016-A; and by CXO through grant No. TM2-23005X. Support for P.F.H. and S.P. was provided by NSF Research grants 1911233, 20009234, 2108318, NSF CAREER grant 1455342, and NASA grant Nos. 80NSSC18K0562 and HST-AR-15800. D.A.A. acknowledges support by NSF grants AST-2009687 and AST-2108944, CXO grant No. TM2-23006X, JWST grant Nos. GO-01712.009-A and AR-04357.001-A, Simons Foundation Award CCA-1018464, and Cottrell Scholar Award CS-CSA-2023-028 by the Research Corporation for Science Advancement. J.M. is funded by the Hirsch Foundation. N.A.W. was supported by a CIERA Postdoctoral Fellowship. Numerical calculations were run on the Caltech computer cluster Wheeler; the Northwestern computer cluster Quest; Frontera allocation FTA-Hopkins/AST20016 supported by the NSF and TACC; XSEDE allocations ACI-1548562, TGAST140023, and TG-AST140064; and NASA HEC allocations SMD-16-7561, SMD-17-1204, and SMD-16-7592. Some figures were generated with the help of FIRE Studio, an open-source Python visualization package (Gurvich 2022).

Data Availability

The data supporting the plots within this article are available on reasonable request to the corresponding author. A public version of the GIZMO code is available at http://www.tapir.caltech.edu/~phopkins/Site/GIZMO.html. Additional data including simulation snapshots, initial conditions, and derived data products are available at http://fire.northwestern.edu/data/.

ORCID iDs

Lindsey Byrne https://orcid.org/0000-0002-8408-1834
Claude-André Faucher-Giguère https://orcid.org/0000-0002-4900-6628
Sarah Wellons https://orcid.org/0000-0002-3977-2724
Philip F. Hopkins https://orcid.org/0000-0003-3729-1684
Daniel Anglés-Alcázar https://orcid.org/0000-0001-5769-4945
Imran Sultan https://orcid.org/0000-0003-2341-1534
Nastasha Wijers https://orcid.org/0000-0001-6374-7185
Jorge Moreno https://orcid.org/0000-0002-3430-3232
Sam Ponnada https://orcid.org/0000-0002-7484-2695

References

Abadi, M. G., Navarro, J. F., Steinmetz, M., & Eke, V. R. 2002, ApJ, 597, 21
Anglés-Alcázar, D., Davé, R., Faucher-Giguère, C. A., Özel, F., & Hopkins, P. F. 2017a, MNRAS, 464, 2840
Anglés-Alcázar, D., Faucher-Giguère, C.-A., Quataert, E., et al. 2017b, MNRAS: Letters, 472, L109
Anglés-Alcázar, D., Özel, F., & Davé, R. 2013, ApJ, 770, 5
Anglés-Alcázar, D., Quataert, E., Hopkins, P. F., et al. 2021, ApJ, 917, 53
Baldry, I. K., Driver, S. P., Loveday, J., et al. 2012, MNRAS, 421, 621
Behroozi, P., Wechsler, R. H., Hearin, A. P., & Conroy, C. 2019, MNRAS, 488, 3143
Bower, R. G., Schaye, J., Frenk, C. S., et al. 2017, MNRAS, 465, 32
Butsky, I. S., Nakum, S., Ponnada, S. B., et al. 2023, MNRAS, 521, 2477
Byrne, L., Faucher-Giguère, C. A., Stern, J., et al. 2023, MNRAS, 520, 722
Cannarozzo, C., Leauthaud, A., Oyarzún, G. A., et al. 2023, MNRAS, 520, 5651
Chan, T. K., Kereš, D., Hopkins, P. F., et al. 2019, MNRAS, 488, 3716
Choi, E., Brennan, R., Somerville, R. S., et al. 2020, ApJ, 904, 8
Choi, E., Ostriker, J. P., Naab, T., et al. 2017, ApJ, 844, 31
Choi, E., Somerville, R. S., Ostriker, J. P., Naab, T., & Hirschmann, M. 2018, ApJ, 866, 91
Choi, E., Somerville, R. S., Ostriker, J. P., Hirschmann, M., & Naab, T. 2024, ApJ, 964, 54
Cicone, C., Maiolino, R., Sturm, E., et al. 2014, A&A, 562, A21
Ciotti, L., & Ostriker, J. P. 2007, ApJ, 665, 1038
Ciotti, L., Ostriker, J. P., Gan, Z., et al. 2022, ApJ, 933, 154
Ciotti, L., Ostriker, J. P., & Proga, D. 2010, ApJ, 717, 708
Cochrane, R. K., Anglés-Alcázar, D., Mercedes-Feliz, J., et al. 2023, MNRAS, 523, 2409
Crain, R. A., & Voort, F. v. d. 2023, ARA&A, 61, 473
Croton, D. J., Springel, V., White, S. D. M., et al. 2006, MNRAS, 365, 11
Davé, R., Anglés-Alcázar, D., Narayanan, D., et al. 2019, MNRAS, 486, 2827
Davies, J. J., Crain, R. A., Oppenheimer, B. D., & Schaye, J. 2020, MNRAS, 491, 4462
de Vaucouleurs, G. 1948, AnAp, 11, 247
Di Matteo, T., Angles-Alcazar, D., Shankar, F., et al. 2023, arXiv:2304.11541
Di Matteo, T., Springel, V., & Hernquist, L. 2005, Natur, 433, 604
Dubois, Y., Devriendt, J., Slyz, A., & Teyssier, R. 2012, MNRAS, 420, 2662
Dubois, Y., Gavazzi, R., Peirani, S., & Silk, J. 2013, MNRAS, 433, 3297
Dubois, Y., Peirani, S., Pichon, C., et al. 2016, MNRAS, 463, 3948
Faber, S. M., & Jackson, R. E. 1976, ApJ, 204, 668
Fabian, A. C. 2012, ARA&A, 50, 455
Faucher-Giguère, C.-A., & Quataert, E. 2012, MNRAS, 425, 605
Faucher-Giguère, C.-A., Quataert, E., & Murray, N. 2012, MNRAS, 420, 1347
Ferrarese, L., & Merritt, D. 2000, ApJL, 539, L9
Feruglio, C., Maiolino, R., Piconcelli, E., et al. 2010, A&A, 518, L155
Fiore, F., Feruglio, C., Shankar, F., et al. 2017, A&A, 601, A143
Fischer, J., Sturm, E., González-Alfonso, E., et al. 2010, A&A, 518, L41
Flores Velázquez, J. A., Gurvich, A. B., Faucher-Giguère, C. A., et al. 2021, MNRAS, 501, 4812
Frigo, M., Naab, T., Hirschmann, M., et al. 2019, MNRAS, 489, 2702
Gallazzi, A., Charlot, S., Brinchmann, J., & White, S. D. 2006, MNRAS, 370, 1106
Gebhardt, K., Bender, R., Bower, G., et al. 2000, ApJL, 539, L13
Girichidis, P., Pfrommer, C., Hanasz, M., & Naab, T. 2020, MNRAS, 491, 993
Greene, J. E., Strader, J., & Ho, L. C. 2020, ARA&A, 58, 257
Gurvich, A. B. 2022, FIRE Studio, Astrophysics Source Code Library, ascl:2202.006
Gurvich, A. B., Stern, J., Faucher-Giguère, C. A., et al. 2023, MNRAS, 519, 2598
Habouzit, M., Volonteri, M., & Dubois, Y. 2017, MNRAS, 468, 3935
Harrison, C. M. 2017, NatAs, 1, 0165
Hopkins, P. F. 2015, MNRAS, 450, 53
Hopkins, P. F. 2016, MNRAS, 462, 576
Hopkins, P. F., Butsky, I. S., Panopoulou, G. V., et al. 2022a, MNRAS, 516, 3470
Hopkins, P. F., Chan, T. K., Garrison-Kimmel, S., et al. 2020a, MNRAS, 492, 3465
Hopkins, P. F., Chan, T. K., Ji, S., et al. 2021, MNRAS, 501, 3640
Hopkins, P. F., Grudić, M. Y., Wetzel, A., et al. 2020b, MNRAS, 491, 3702
Hopkins, P. F., Hernquist, L., Cox, T. J., Robertson, B., & Krause, E. 2007, ApJ, 669, 45
Hopkins, P. F., Kereš, D., Oñorbe, J., et al. 2014, MNRAS, 445, 581
Hopkins, P. F., Murray, N., Quataert, E., & Thompson, T. A. 2010, MNRAS, 401, L19
Hopkins, P. F., & Quataert, E. 2011, MNRAS, 415, 1027
Hopkins, P. F., & Raives, M. J. 2016, MNRAS, 455, 51
Hopkins, P. F., Squire, J., Butsky, I. S., & Ji, S. 2022b, MNRAS, 517, 5413
Hopkins, P. F., Squire, J., & Butsky, I. S. 2021, MNRAS, 509, 3779
Hopkins, P. F., Torrey, P., Faucher-Giguère, C.-A., Quataert, E., & Murray, N. 2016, MNRAS, 458, 816
Hopkins, P. F., Wellons, S., Angles-Alcázar, D., Faucher-Giguère, C. A., & Grudić, M. Y. 2022c, MNRAS, 510, 630
Hopkins, P. F., Wetzel, A., Kereš, D., et al. 2018, MNRAS, 480, 800
Hopkins, P. F., Wetzel, A., Wheeler, C., et al. 2023, MNRAS, 519, 3154
Ji, S., Chan, T. K., Hummels, C. B., et al. 2020, MNRAS, 496, 4221
Ji, S., Kereš, D., Chan, T. K., et al. 2021, MNRAS, 505, 259
Lauer, T. R., Gebhardt, K., Faber, S. M., et al. 2007, ApJ, 664, 226
Leitherer, C., Schaerer, D., Goldader, J. D., et al. 1999, ApJS, 123, 3
Liu, G., Zakamska, N. L., Greene, J. E., Nesvadba, N. P. H., & Liu, X. 2013, MNRAS, 436, 2576
Magorrian, J., Tremaine, S., Richstone, D., et al. 1998, AJ, 115, 2285
Mercedes-Feliz, J., Angles-Alcázar, D., Hayward, C. C., et al. 2023, MNRAS, 524, 3446
Mercedes-Feliz, J., Anglés-Alcázar, D., Oh, B. K., et al. 2024, MNRAS, 530, 2795
Moe, M., Arav, N., Bautista, M. A., & Korista, K. T. 2009, ApJ, 706, 525
Muzzin, A., Marchesini, D., Stefanon, M., et al. 2013, ApJ, 777, 18
Naab, T., & Ostriker, J. P. 2017, ARA&A, 55, 59
Nelson, D., Pillepich, A., Springel, V., et al. 2018, MNRAS, 475, 624
Parsotan, T., Cochrane, R. K., Hayward, C. C., et al. 2021, MNRAS, 501, 1591
Peng, Y. J., Lilly, S. J., Kovač, K., et al. 2010, ApJ, 721, 193
Planck Collaboration, Aghanim, N., Akrami, Y., et al. 2020, A&A, 641, A6
Power, C., Navarro, J. F., Jenkins, A., et al. 2003, MNRAS, 338, 14
Remus, R.-S., & Forbes, D. A. 2022, ApJ, 935, 37
Richings, A. J., & Faucher-Giguère, C.-A. 2018, MNRAS, 478, 3100
Richings, A. J., & Faucher-Giguère, C.-A. 2018, MNRAS, 474, 3673
Richings, A. J., Faucher-Giguère, C.-A., & Stern, J. 2021, MNRAS, 503, 1568
Rosito, M. S., Pedrosa, S. E., Tissera, P. B., et al. 2021, A&A, 652, A44
Rosito, M. S., Tissera, P. B., Pedrosa, S. E., & Rosas-Guevara, Y. 2019, A&A, 629, A37
Rupke, D. S. N., & Veilleux, S. 2013, ApJL, 775, L15
Ruszkowski, M., Yang, H.-Y. K., & Zweibel, E. 2017, ApJ, 834, 208
Salim, S., Rich, R. M., Charlot, S., et al. 2007, ApJS, 173, 267
Scannapieco, C., Tissera, P. B., White, S. D. M., & Springel, V. 2008, MNRAS, 389, 1137
Schaye, J., Crain, R. A., Bower, R. G., et al. 2015, MNRAS, 446, 521
Shakura, N. I., & Sunyaev, R. A. 1973, A&A, 24, 337
Sijacki, D., Springel, V., Di Matteo, T., & Hernquist, L. 2007, MNRAS, 380, 877
Silk, J., & Rees, M. J. 1998, A&A, 331, L1
Somerville, R. S., & Davé, R. 2015, ARA&A, 53, 51
Somerville, R. S., Hopkins, P. F., Cox, T. J., Robertson, B. E., & Hernquist, L. 2008, MNRAS, 391, 481
Springel, V., Di Matteo, T., & Hernquist, L. 2005, ApJL, 620, L79

Stern, J., Faucher-Giguère, C.-A., Fielding, D., et al. 2021, ApJ, 911, 88
Sturm, E., González-Alfonso, E., Veilleux, S., et al. 2011, ApJL, 733, L16
Su, K.-Y., Bryan, G. L., Hayward, C. C., et al. 2024, MNRAS, 532, 2724
Su, K.-Y., Hopkins, P. F., Bryan, G. L., et al. 2021, MNRAS, 507, 175
Su, K.-Y., Hopkins, P. F., Hayward, C. C., et al. 2019, MNRAS, 487, 4393
Su, K.-Y., Hopkins, P. F., Hayward, C. C., et al. 2020, MNRAS, 491, 1190
Terrazas, B. A., Bell, E. F., Pillepich, A., et al. 2020, MNRAS, 493, 1888
Thomas, T., & Pfrommer, C. 2019, MNRAS, 485, 2977
Tomczak, A. R., Quadri, R. F., Tran, K. V. H., et al. 2014, ApJ, 783, 85
Torrey, P., Hopkins, P. F., Faucher-Giguère, C.-A., et al. 2020, MNRAS, 497, 5292
Tremmel, M., Karcher, M., Governato, F., et al. 2017, MNRAS, 470, 1121
Weinberger, R., Springel, V., Hernquist, L., et al. 2017, MNRAS, 465, 3291
Weinberger, R., Springel, V., Pakmor, R., et al. 2018, MNRAS, 479, 4056
Weinberger, R., Su, K. Y., Ehlert, K., et al. 2023, MNRAS, 523, 1104
Wellons, S., Faucher-Giguère, C. A., Anglés-Alcázar, D., et al. 2020, MNRAS, 497, 4051
Wellons, S., Faucher-Giguère, C. A., Hopkins, P. F., et al. 2023, MNRAS, 520, 5394
Yoon, D., Yuan, F., Ostriker, J. P., Ciotti, L., & Zhu, B. 2019, ApJ, 885, 16
Zweibel, E. G. 2013, PhPl, 20, 055501
Zweibel, E. G. 2017, PhPl, 24, 055402